Neutron Skin of Na Isotopes Studied via Their Interaction Cross Sections

T. Suzuki,[1,2] H. Geissel,[2] O. Bochkarev,[3] L. Chulkov,[3] M. Golovkov,[3] D. Hirata,[1] H. Irnich,[2] Z. Janas,[2] H. Keller,[2] T. Kobayashi,[1] G. Kraus,[2] G. Münzenberg,[2] S. Neumaier,[2] F. Nickel,[2] A. Ozawa,[1] A. Piechaczeck,[2] E. Roeckl,[2] W. Schwab,[2] K. Sümmerer,[2] K. Yoshida,[1] and I. Tanihata[1]

[1]*RIKEN (The Institute for Physical and Chemical Research), 2-1 Hirosawa, Wako, Saitama 351-01, Japan*
[2]*Gesellschaft für Schwerionenforschung, Planckstrasse 1, D-64291 Darmstadt, Germany*
[3]*Kurchatov Institute, Kurchatov sq. 1, 123182, Moscow, Russia*

(Received 14 August 1995)

The interaction cross sections (σ_I) of ^{A}Na isotopes ($A = 20-23, 25-32$) on a carbon target have been measured at 950A MeV. The effective root-mean-square matter radii of these isotopes were deduced from σ_I by a Glauber-type calculation. By combining the isotope-shift data with the present data the radii of neutrons have been compared with those of protons for the first time along a chain of stable and unstable isotopes. A monotonic increase in the neutron skin thickness has been observed as the neutron number increases in Na isotopes.

PACS numbers: 21.10.Gv, 25.60.+v, 27.30.+t

How large a difference can be seen between the proton and neutron density distributions in unstable nuclei? This question is of basic interest among new structure phenomena concerning exotic nuclei. The presence of a neutron skin in stable nuclei has been discussed since the mid 1950s [1]. No evidence of a thick neutron skin in stable nuclei has been observed, even if many of them have a large neutron excess ($N - Z$) [2]. Recently, thick neutron skins with a thickness of 0.9 fm have been reported by Tanihata *et al.* in the He isotopes [3]. They used a relation [4] between the interaction cross sections (σ_I) and the nucleon-removal cross sections to draw their conclusion, since there is no measurement for the charge or proton distribution in those nuclei. Therefore, the result was model dependent. A unique opportunity to compare nuclear matter and charge radii over a wide range of neutron numbers, however, lies in Na isotopes. The rms charge radii ($\tilde{r}_c \equiv \langle r_c^2 \rangle^{1/2}$) have been determined by isotope-shift measurements [5]. To obtain more direct information concerning the neutron skin, we measured σ_I, determined the effective rms matter radii ($\tilde{r}_m \equiv \langle r_m^2 \rangle^{1/2}$), and deduced the rms neutron radii ($\tilde{r}_n \equiv \langle r_n^2 \rangle^{1/2}$) for a chain of Na isotopes in the mass range from $A = 20$ to 32.

The experiment was performed at the Projectile Fragment Separator (FRS) facility at GSI. Secondary beams of $^{20-23}$Na and $^{25-32}$Na at 950A MeV were produced through the projectile fragmentation of ^{36}Ar and ^{40}Ar primary beams, respectively, accelerated by the heavy-ion synchroton SIS. A maximum beam intensity of 2×10^9 particles per spill was used to produce ^{31,32}Na. Figure 1(a) shows a schematic view of the experimental setup. The primary beam energies and the thickness of the Be production targets (1006 and 4009 mg/cm^2) were adjusted isotope by isotope so that the nucleon per energies of the secondary Na beams at the middle of the reaction targets could be equal within ± 8 MeV. The first half of the FRS, down to the intermediate focal plane (F2), was used to separate and identify the incident Na beams. Reaction targets of C with 7.428 and 3.715 g/cm^2 in thickness were placed at F2. The uniformity of the targets in thickness was better than 0.01%. Position-sensitive scintillation detectors

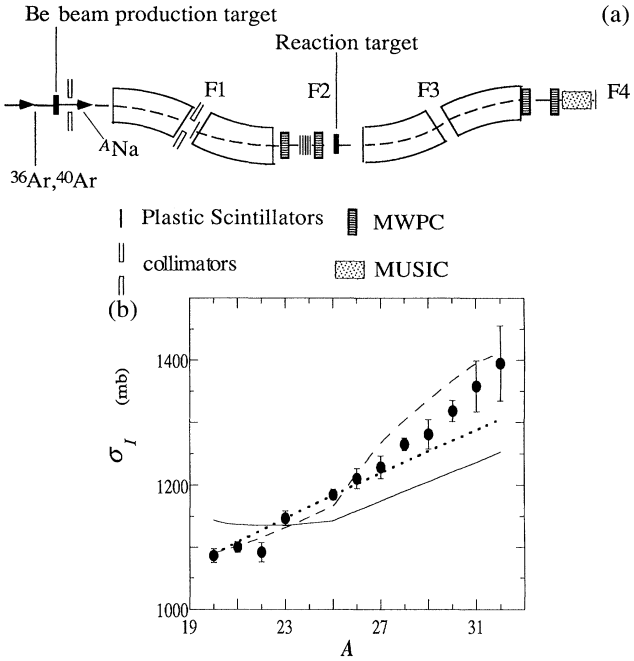

FIG. 1. (a) Experimental setup for measuring the interaction cross sections at FRS in GSI. (b) Interaction cross sections (σ_I) for Na isotopes on carbon targets at 950A MeV. The dotted line indicates the σ_I calculated by Eq. (1). The dashed (solid) line shows the σ_I calculated by the Glauber model. The density distribution used was obtained from the RMF model for both a proton and a neutron in the case of the dashed line, while the neutron density distribution was assumed to be the same as that of a proton, except for the normalization (N/Z) in the solid line. See text.

were placed at F1, F2, and F4 and a multisampling ion chamber (MUSIC) was placed at F4. They provided particle identification via time-of-flight (TOF), magnetic rigidity ($B\rho$), and energy-deposition (ΔE) measurements in front of and behind the reaction targets. In both sections the ΔE resolution [$\sigma(Z) = 0.18$ at F2, 0.15 at F4] and the TOF resolution [σ(TOF) = 100 ps] were sufficient to unambiguously identify the nuclear mass (A) and charge (Z) for each beam particle. The relative amount of contaminants was estimated to be less than 0.1%. The second half of the FRS was used as a spectrometer to transport the noninteracting nuclei down to the final focus, where the noninteracting Na nuclei in the target were identified and counted, thus providing a measurement of σ_I by the transmission method. The σ_I was then calculated by the equation $\sigma_I = (1/N_t)\ln(\Gamma_0/\Gamma)$, where Γ is the ratio of the number of noninteracting nuclei to that of incoming nuclei for a target-in run, and Γ_0 is the same ratio for an empty-target run. The number of target nuclei per unit area is denoted as N_t. The values of Γ_0 were larger than 0.86, and Γ were 0.49–0.61 (0.64–0.76) for a thick (thin) target. The deviation of Γ_0 from unity was mainly due to nuclear reactions in the detectors. The momentum and angular emittance guaranteed full transmission in the second section for noninteracting Na particles. This was studied using the simulation code MOCADI [6], which took into account the effect of fragmentations and small-angle deflections due to multiple Coulomb scattering in the reaction target. Actually, it was achieved as follows: (i) operating the FRS in an optical mode which resulted in smaller vertical envelopes at focal planes F1 and F3, (ii) limiting the incident transverse emittance at F1, and (iii) restricting the beam emittance in an off-line analysis by ray tracing with the multiwire proportional chambers (MWPC) located at F2. The thus-determined σ_I and the interaction radii (R_I) defined in Ref. [7] are listed in Table I.

In Fig. 1(b) the σ_I are plotted as a function of the mass number of Na isotopes. The dotted line in the figure shows the σ_I calculated by the equation

$$\sigma_I = \pi[R_I(\mathrm{C}) + r_0 A^{1/3}]^2, \quad (1)$$

where R_I(C) is the interaction radius of ^{12}C (2.61 fm) and r_0 is so selected as to reproduce the ^{23}Na cross section. It can be seen that the increase in the cross section is faster than that expected from this simple mass dependence.

The solid line in Fig. 1(b) shows the σ_I obtained by a Glauber-model calculation [8] under the assumption that the neutron-density distribution has the same shape as that of protons, except for a scaling factor (N/Z). The proton-density distribution used for the calculation was derived from a relativistic mean field model (RMF) [9] that includes axial deformation. Using the TM1 parameter set [10], this model reproduces the binding energies [11] and the $\tilde{r}_c$ of Na isotopes very well. It also reproduces the observed prolate deformation of $^{21-24,28-31}$Na. The density distribution of ^{12}C used was the harmonic-oscillator (HO) distribution. The width of the HO distribution was set so as to be consistent with the known σ_I(C + C) [12] as well as the $\tilde{r}_c$ obtained from electron scattering. It is clearly seen that the measured cross sections are much larger than the solid line at the neutron-rich side, and smaller at the proton-rich side. It therefore shows a gradual growth of the neutron skin for neutron-rich Na isotopes, and a possible proton skin for proton-rich isotopes. The dashed line in Fig. 1(b) shows the σ_I obtained with the density distribution using the RMF density distributions (both proton and neutron), which exhibits thick neutron skins in Na isotopes. It agrees very well with the data. In all comparisons it qualitatively indicates that the neutron densities spread much wider than that of a proton for neutron-rich Na isotopes.

TABLE I. Interaction cross sections (σ_I) in millibarns, interaction radii (R_I), and nuclear effective rms radii in fm.

A	σ_I [a]	R_I [b]	$\tilde{r}_p$ [c]	$\tilde{r}_n$ Case (a)	$\tilde{r}_n$ Case (b)
20	1086 (11)	3.27 (5)	2.806 (15)	2.737 (84)	2.715 (84)
21	1100 (9)	3.31 (4)	2.862 (12)	2.685 (55)	2.663 (63)
22	1092 (16)	3.29 (8)	2.829 (11)	2.642 (82)	2.57 (11)
23	1147 (12)	3.43 (5)	2.829 (9)	2.867 (55)	2.867 (68)
25	1185 (9)	3.53 (4)	2.794 (10)	2.968 (32)	2.970 (43)
26	1211 (16)	3.60 (8)	2.814 (10)	3.015 (53)	3.028 (77)
27	1229 (18)	3.65 (9)	2.836 (11)	3.034 (59)	3.047 (86)
28	1265 (10)	3.74 (4)	2.862 (12)	3.109 (32)	3.145 (46)
29	1281(22)	3.78 (10)	2.919 (16)	3.106 (65)	3.141 (92)
30	1318 (15)	3.87 (7)	2.942 (21)	3.184 (39)	3.240 (67)
31	1358 (41)	3.97 (20)	2.985 (14)	3.25 (11)	3.37 (16)
32	1395 (61)	4.05 (30)		3.32 (16)	3.43 (21)

[a]Errors include both statistical and systematic errors.
[b]Interaction radius R_I is defined as $\sigma_I = \pi[R_I(^A\mathrm{Na}) + R_I(\mathrm{C})]^2$, where R_I(C) = 2.61 fm.
[c]Data were taken from Ref. [5] using the relation $\tilde{r}_p^2 = \tilde{r}_c^2 - 0.64$.

In the following we use the Glauber model to obtain a quantitative comparison between the effective rms neutron radius and the rms proton radius. We applied the optical limit of the Glauber model to obtain the effective rms radii ($\tilde{r}_k$). Subscript k denotes p (c) for the proton (charge) distribution or n (m) for the neutron (matter) distribution, respectively. These quantities are connected by the relation $\tilde{r}_m^2 = (Z/A)\tilde{r}_p^2 + (N/A)\tilde{r}_n^2$, where $\tilde{r}_p$ ($\tilde{r}_n$) is the point proton (neutron) radius, i.e., $\tilde{r}_p^2 = \tilde{r}_c^2 - 0.64$. It is well established that the Glauber model predicts the experimental data with a few percent accuracy using elementary N-N cross sections and the known nuclear-density distribution between stable nuclei at high energy [7]. As for the form of the density distribution of projectiles, we used the Fermi-type distribution for both protons and neutrons. Namely, the density $\rho_k(r)$ at a distance r is given by

$$\rho_k(r) = \frac{\rho_k(0)}{1 + \exp[(r - R_k)/d_k]}, \qquad (2)$$

where the parameter R_k is the half-density radius and d_k is the surface diffuseness. Subscript k indicates a proton or neutron. It was found that the Fourier transformation of the longitudinal form factor $[|F_L(q)|]$, measured in elastic electron scattering on ^{23}Na [13], could be well fitted by the above equation for $r < 4.0$ fm, while the covered range of the momentum transfer (q) was limited as $0.25 < q < 2$ fm^{-1}. The fitted parameters for the proton distribution in ^{23}Na ($R_p = 3.137$ fm, $d_p = 0.564$ fm) gave the value $\tilde{r}_p = 2.829$ fm, which agrees with $\tilde{r}_p$ obtained from the experimental value of $\tilde{r}_c$ [14].

There are four parameters (R_p, R_n, d_p, and d_n) in these distributions. On the other hand, only two quantities were experimentally determined. Therefore, we have to assume further conditions between the parameters in order to deduce the density distribution or the effective rms radius. To see the sensitivity of the assumption to the final results, we applied two extreme assumptions: (a) $R_n(^A\text{Na}) = r_0 N^{1/3}$ and $R_p(^A\text{Na}) = R_n(^{23}\text{Na}) = 3.137$ fm (the value obtained for ^{23}Na), and (b) $d_p(^A\text{Na}) = d_n(^A\text{Na}) = 0.564$ fm (the value obtained at ^{23}Na). In assumption (a), the densities are considered to change only due to changes in the surface diffuseness, except for the $N^{1/3}$ dependence of R_n. On the other hand, all changes are put into changes of R_k in assumption (b). We consider that a realistic change would be somewhere in between these two assumptions. The resultant $\tilde{r}_n$ are listed in Table I together with $\tilde{r}_p$ from $\tilde{r}_c$. The value of $\tilde{r}_m$ for the stable nuclei ^{23}Na (2.85 $\pm$ 0.03 fm) agrees well with the value of 2.82 $\pm$ 0.12 fm determined through ^{3}He elastic scattering at Orsay [15] within error bars. As the third case, we assumed that ρ_Z and ρ_N are similar to each other, except for the N/Z ratio in its normalization. This expression corresponds to a skinless limit, and has only two parameters [$R_p(^A\text{Na}) = R_n(^A\text{Na}) = r_0 A^{1/3}$ and $d_p(^A\text{Na}) = d_n(^A\text{Na})$]. The parameters were searched to fit to both experimental $\tilde{r}_m$ ($= \tilde{r}_c$, in this case) and the σ_I for $20 \leq A \leq 30$. It was impossible to fit by fixing the r_0 (0.87) determined in the case of ^{23}Na. The resultant parameters behave quite unphysically against the neutron number. We therefore cannot accept this skinless limit.

In Fig. 2 these empirical values of $\tilde{r}_n$ from cases (a) and (b) are plotted against the neutron number together with the values of $\tilde{r}_p$. It indicates a gradual growth of the thickness of the neutron skin ($\Delta R \equiv \tilde{r}_n - \tilde{r}_p$) for neutron-rich Na isotopes up to 0.4 fm. The value of 0.4 fm is much larger than the observation in neutron-rich β-stable ^{48}Ca (0.12 fm) [16]. It is seen that the RMF calculation reproduces the tendency of experimental data well, as well as the thickness of a neutron skin of 0.4 fm for $A = 32$. At $N = 11$, $\tilde{r}_n$ seems to deviate from the solid line reflecting its relatively small σ_I. This might be due to the mixture of the isomer state in ^{22}Na. Since the flight time ($\sim$138 ns) from the production target to F2 is shorter than the half-life of the isomer (243 ns), the contribution may not be negligible.

The deduction of $\tilde{r}_c$ based on the isotope shift requires an empirical factor ζ (so-called isotope-shift discrepancy) in evaluating the mass-effect constant, because there is only one stable Na isotope. We thus examined how a change in ζ affects the thickness of the neutron skin using Fig. 11 of Ref. [5], where the values of $\tilde{r}_c$ corresponding to the $\zeta = 1.0$ case are presented together with the $\zeta = 0.5$ case as the upper and lower limits, respectively. The change of $\zeta = 1.0$ from $\zeta = 0.5$ decreases the thickness of the neutron skin in ^{32}Na from 0.4 down to 0.2 fm, while it does not change very much in ^{20}Na. As Ref. [5] pointed out, ζ is generally found to be around 0.5; we thus took the values of $\tilde{r}_c$ corresponding to $\zeta = 0.5$. It is also

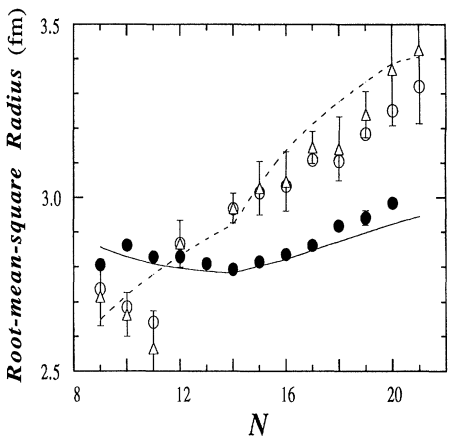

FIG. 2. The rms neutron radii ($\tilde{r}_n$) [open circles from case (a), open triangles from case (b)] and the rms proton radii ($\tilde{r}_p$) (solid circles) from Ref. [5] as a function of the neutron number of Na isotopes. The error bars for the $\tilde{r}_n$ are shown only for case (b). The dashed (solid) line is the calculated $\tilde{r}_n$ ($\tilde{r}_p$) by the RMF model.

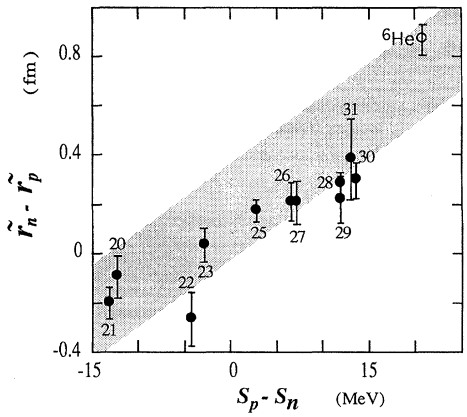

FIG. 3. The two-dimensional plot of the difference between the proton separation energy and that of a neutron ($S_p - S_n$) versus the thickness of the neutron skin ($\tilde{r}_n - \tilde{r}_p$). The corresponding mass number is indicated at each data point. The shaded area shows the calculated correlation for various isotopes ranging from helium up to lead. The datum of ^{6}He from Ref. [3] is also plotted for a comparison, where the mass excess of ^{5}H was taken from Ref. [19].

seen that the RMF calculation agrees much better for the $\tilde{r}_p$ determined by $\zeta = 0.5$.

In the following we restrict ourselves to a discussion based on the result from case (b); however, the discussion does not differ if we use case (a). In Fig. 3 ΔR is plotted against the difference between the neutron and proton separation energy or the Fermi-energy difference ($S_p - S_n$). For nuclei having an even neutron number, we took S_n as half of the two-neutron separation energy. Here, S_p and S_n were calculated from the mass excess given in Refs. [17] and [18]. It can be seen that ΔR has a strong correlation with $S_p - S_n$, for the first time. Such a correlation has been predicted by the RMF model [3], and is shown by the shadow in the figure. The experimental data agree well with the prediction.

In summary, we have measured σ_I of $^{20-23,25-32}$Na. The observed mass dependence of σ_I is much stronger than that expected from a prediction which assumes no neutron skin. It has therefore shown the growth of the neutron skin in neutron-rich isotopes of Na. The data were analyzed using a Glauber-type model, and the effective rms neutron radii were deduced. Combining the isotope-shift data with the present data, $\tilde{r}_n$ was compared with $\tilde{r}_p$ for the first time, along a long chain including unstable nuclei. This indicates a gradual growth of the neutron skin for neutron-rich β-unstable Na isotopes up to 0.4 fm. It is important to check in other nuclei as to whether the neutron skin is considered to be a common structure that appears in neutron-rich β-unstable nuclei or not. Further experiments at different incident beam energy are desired in order to determine the density distribution of both protons and neutrons in a model-independent way.

We would like to thank the members of the FRS group and the SIS staff members for their help and K. H. Behr, A. Bruenle, and K. Burkard for their technical assistance. Thanks also go to M. Fukuda for stimulating discussions. One of the authors (T. S.) gratefully acknowledges the financial support of GSI.

[1] W. D. Myers and W. J. Swiatecki, Ann. Phys. (N.Y.) **55**, 395 (1969).
[2] C. J. Batty *et al.*, Adv. Nucl. Phys. **19**, 1 (1989).
[3] I. Tanihata *et al.*, Phys. Lett. B **289**, 261 (1992).
[4] Y. Ogawa *et al.*, Nucl. Phys. **A539**, 295 (1992).
[5] G. Huber *et al.*, Phys. Rev. C **18**, 2342 (1978).
[6] Th. Schwab, GSI Report No. 91-10, 1991 (unpublished).
[7] I. Tanihata *et al.*, Phys. Rev. Lett. **55**, 2676 (1985).
[8] G. F. Bertsch *et al.*, Phys. Rev. C **39**, 1154 (1989).
[9] D. Hirata *et al.*, Phys. Rev. C **44**, 1467 (1991).
[10] Y. Sugahara and H. Toki, Nucl. Phys. **A579**, 557 (1994).
[11] C. Thibault *et al.*, Phys. Rev. C **12**, 644 (1975).
[12] S. Shimoura *et al.*, in *Proceedings of the First International Conference on Radioactive Nuclear Beams,* edited by W. D. Meyers, J. M. Nitschke, and E. B. Norman (World Scientific, Singapore, 1989), p. 439.
[13] R. P. Singhal *et al.*, J. Phys. G **8**, 1059 (1982).
[14] H. de Vries, C. W. de Jager, and C. de Vries, At. Data Nucl. Data Tables **36**, 495 (1987).
[15] V. Vernotte *et al.*, Nucl. Phys. **A390**, 285 (1982).
[16] W. R. Gibbs and J.-P. Dedonder, Phys. Rev. C **46**, 1825 (1992).
[17] P. M. Endt, Nucl. Phys. **A521**, 1 (1990).
[18] N. A. Orr *et al.*, Phys. Lett. B **258**, 29 (1991).
[19] G. Audi and A. H. Wapstra, Nucl. Phys. **A565**, 1 (1993).